European Journal of Radiology 117 (2019) 164–170

Contents lists available at ScienceDirect

European Journal of Radiology

journal homepage: www.elsevier.com/locate/ejrad

Research article

Magnetic resonance texture analysis for the identification of cytokeratin 19-positive hepatocellular carcinoma

He-qing Wang[a,b,1], Chun Yang[a,1], Meng-su Zeng[a], Sheng-xiang Rao[a], Yuan Ji[c], Xin Weng[d], Ji-yong Wang[d], Ruo-fan Sheng[a,*]

[a] Department of Radiology, Zhongshan Hospital, Fudan University, Shanghai Institute of Medical Imaging, No. 180 Fenglin Road, Xuhui District, Shanghai, 200032, China
[b] Department of Radiology, First Affiliated Hospital of Dalian Medical University, No. 222 Zhongshan Road, Xigang District, Dalian, 116011, China
[c] Department of Pathology, Zhongshan Hospital, Fudan University, No. 180 Fenglin Road, Xuhui District, Shanghai, 200032, China
[d] Shanghai United Imaging Healthcare Co., Ltd. No. 2258 Chengbei Road, Jiading District, Shanghai, 201815, China

ARTICLE INFO

Keywords:
Hepatocellular carcinoma
Cytokeratin 19
Magnetic resonance imaging
Texture

ABSTRACT

Purpose: To investigate potential findings associated with cytokeratin 19 (CK19)-positive HCC, with special emphasis on MR texture analysis.

Materials and methods: Forty-eight patients with CK19-negative HCC and 38 patients with CK19-positive were retrospectively evaluated by texture analysis based on conventional MRI. Clinicalpathological characteristics, conventional MR imaging findings, and the MR texture analysis contained of 2415 texture features in the seven conventional sequences were compared. Significant features for differentiating were identified by univariate and multivariate analyses. Receiver operating characteristic analyses of the significant findings were performed and compared to evaluate their diagnostic performance.

Results: There was no significant difference between the top1 texture feature (three-dimensional standard deviation separation of intensity on T2-weighted original images, abbreviated as: StdSeparation 3D) and the combined top1-6 feature in identifying CK19-positive HCC($P = 0.660$). Univariate and multivariate analyses indicated that serum alpha-fetoprotein (AFP) level ≥ 400 ng/mL($P = 0.013$), arterial rim enhancement ($P = 0.005$), and StdSeparation 3D texture character($P = 0.002$) were independent variables associated with CK19-positive HCCs. The combination of the three indices showed a better performance than AFP level ($P = 0.0028$), arterial rim enhancement($P < 0.0001$), and their combination($P = 0.0098$); while no significantly better than the StdSeparation 3D texture character alone($P = 0.0788$). An acceptable discrimination (AUC = 0.765) with both sensitivity and specificity greater than 75% was achieved for StdSeparation 3D texture character.

Conclusion: Serum AFP level ≥ 400 ng/mL, arterial rim enhancement, and the StdSeparation 3D texture character were independently associated with CK19-positive HCC. The StdSeparation 3D texture character may be a reliable imaging biomarker which can improve the diagnostic performance.

1. Introduction

Hepatocellular carcinoma (HCC) is the sixth most common cancer and the third leading cause of cancer death [1]. Despite the development of treatment strategy, high intrahepatic recurrence rate remains a major challenge [2]. HCC expressing progenitor cell markers has a different pathway of hepatic carcinogenesis, and specific morphological and immunophenotypic characteristics, which is considered a novel molecular pathologic entity [3–5]. Among progenitor cell markers of HCC, cytokeratin 19 (CK19) tends to be related to a worse prognosis

Abbreviations: CK19, cytokeratin 19; StdSeparation 3D, three-dimensional standard deviation separation of intensity on T2-weighted original images; AFP, alpha-fetoprotein; HCC, hepatocellular carcinoma; DWI, diffusion weighted imaging; ADC, apparent diffusion coefficient; ROI, region of interest; PACS, picture archiving and communication system; SI, signal intensity; LBP-HF, local binary pattern histogram Fourier; GLCM, gray-level co-occurrence matrix; GLGCM, grey level gradient co-occurrence matrix; SD, standard deviation; ROC, receiver operating characteristic; AUCs, areas under the curve

* Corresponding author at: Department of Radiology, Zhongshan Hospital, Fudan University, No. 180 Fenglin Road, Xuhui District, Shanghai, 200032, China.
E-mail addresses: betteralice@163.com (H.-q. Wang), 15096792@qq.com (C. Yang), raoxray@163.com (S.-x. Rao), ji_yuan2013@126.com (Y. Ji), xin.weng@united-imaging.com (X. Weng), jiyong.wang@united-imaging.com (J.-y. Wang), ruofansheng@163.com (R.-f. Sheng).

[1] He-qing Wang and Chun Yang contribute the same to the article.

https://doi.org/10.1016/j.ejrad.2019.06.016
Received 21 April 2019; Received in revised form 3 May 2019; Accepted 17 June 2019

with a higher rate of recurrence and metastases [4–7]. Thus, identifying HCC with CK19 expression may help to identify the high-risk subgroup, providing clues for individualized therapy.

Until now, few studies have attempted to evaluate the MR imaging findings of HCCs with positive CK19, which all limited to conventional imaging findings [3,8]. Texture analysis, an emerging area of radiomics, provides an objective, quantitative assessment of tumor heterogeneity by analyzing the distribution and relationship of pixel or voxel grey levels in the image, and may reflect information about the tissue microenvironment [9]. We consider it a promising imaging means in the identification of CK19 positive HCC. To our knowledge, there has been no study dealing with the MR texture analysis of HCC related to CK19 expression.

In this study, we aimed to investigate potential findings associated with CK19-positive HCC, with special emphasis on the MR texture analysis, in comparison with CK19-negative HCC.

2. Materials and methods

2.1. Patients

This retrospective study was approved by the institutional review board and informed consent was waived. Patients were identified by searching our institution's pathology database between January and December 2017. The inclusion criteria were (a) pathologically proven HCC after hepatectomy or liver transplantation; (b) abdominal contrast-enhanced MRI performed in our institution following standard protocol prior to surgery; (c) immunochemical staining for CK19. The exclusion criteria were (a) interval longer than 14 days between MRI and surgery; (b) history of prior local-regional therapy; (c) all lesions smaller than 1 cm in diameter; (d) HCCs with tumor in vein or portal vein tumor thrombus at preoperative MR imaging; (e) pathological proven combined HCC and cholangiocarcinoma; (f) poor image quality due to severe susceptibility artifacts or respiratory motion artifacts; (g) diffusive infiltrative lesions. Flowchart of the included and excluded patients is shown in Fig. 1. Clinical characteristics were reviewed by one clinician from patient medical records at our institution.

2.2. Pathological analysis

All HCC specimens were reviewed by one liver pathologist with 20 years of experience. Immunoreactivity was measured as a positive percent area for CK19. In case of multiple tumors, CK19 percentage was reported on a per-lesion basis. To minimize false-positive findings, a cut-off of 5% CK19 cells was regarded as a positive finding ($\geq$ 5% of tumor cells), cases that expressed CK19 in less than 5% of tumor cells were excluded [10].

2.3. Image acquisition

All patients were examined with a 24-channel 1.5 T magnetic scanner (uMR 560; United Imaging Healthcare, Shanghai, China). Routine plain-scan liver protocols consisted of a breath-hold T2-weighted fat-suppressed fast spin-echo sequence, T1-weighted in-phase and opposed-phase gradient echo sequence, and free-breath diffusion weighted imaging (DWI) with a transverse single shot spin-echo echo-planar sequence (b value, 0 and 500 s/mm^2). Dynamic imaging was performed with breath-hold T1-weighted 3-dimensional fat-suppressed gradient-echo, volumetric interpolated body examination sequence, before and after the intravenous administration of gadopentetate dimeglumine (Magnevist; Bayer HealthCare, Berlin, Germany). Gadopentetate dimeglumine was administered at a dose of 0.1 mmol/kg at a rate of 2 mL/s, followed by a 20 mL saline flush using a power injector (Spectris; Medrad, Pittsburgh, PA). The arterial phase acquisition was triggered automatically when contrast media reached the ascending aorta. For subsequent acquisition, dynamic T1-weighted MRI at 60 s (the portal venous phase) and 180 s (the delay phase) was performed [11]. Detailed parameters of each acquisition sequence are shown in Table 1.

2.4. Image analyses

2.4.1. Conventional MR imaging analyses

MR images were retrospectively evaluated using a picture archiving and communication system (PACS; Pathspeed, GE Medical Systems Integrated Imaging Solutions, Prospect, IL, USA). As for multiple nodules, only the largest one was analyzed. Image-pathology matching was performed according to lesion size and location to ensure that the pathological specimen correlated with the lesion evaluated on MRI.

2.4.2. Qualitative analyses

The following qualitative imaging parameters of lesions were evaluated: (a) contour (smooth or irregular: non-smooth margin with budding portion at the tumor periphery); (b) signal intensity (SI) on T1-weighted imaging (T1WI) (hypointensity or iso-hyperintensity); (c) SI on T2-weighted imaging (T2WI) (iso-hypointensity or hyperintensity); (d) lesion homogeneity (homogeneous or heterogeneous on T2WI); (e) target sign on DWI (rim-like hyperintensity with central hypointensity); (f) arterial rim enhancement (ring-like enhancement of the lesion with central hypointensity on arterial phase); (g) enhancement intensity on arterial phase (mild to moderate: less than or equal to portal vein; marked: approximately equal to aorta); (h) dynamic enhancement pattern (progressive: the range or intensity of enhancement progressed over time; persistent: the enhancement remained invariable through all phases; degressive: decreasing hyperintensity over time without hypointense appearance on portal or delayed phases; wash out: the contrast enhancement decreased with hypointensity on portal or delayed phases); (i) enhancing capsule (smooth, uniform border around the tumor with delayed enhancement). All images were assessed in consensus by two radiologists (with 8 and 18 years of experience in abdominal imaging). The reviewers knew that the patients had HCC but were unaware of all other information regarding patients' history, laboratory, and immunochemical pathological results.

2.4.3. Quantitative analyses

A third radiologist (with 10 years of experience in abdominal imaging) performed the quantitative analyses. Lesion size was measured (the maximum dimension) on the axial plane of delayed phase after contrast for which the tumor had the largest cross-sectional diameter.

As for apparent diffusion coefficient (ADC) values, region of interest (ROI) was manually drawn on DWI of the whole lesion as large as possible and the adjacent liver parenchyma using a fixed-sized circular ROI of 100 mm^2, great care was taken to avoid large vessels, necrosis, hemorrhage, and artifacts. These ROIs were then copied onto the ADC maps, and the ADC values were assessed. For each case, 3 ROIs were placed on 3 subsequent slice locations and the average value was used. Ratios of the tumor-to-liver ADC were also recorded.

2.5. MR texture analyses

2.5.1. Image pre-processing

The image pre-processing stage included the slice selection and gray-level normalization. First, ROI was manually drawn by a radiologist (with 10 years of experience in abdominal imaging) over the whole lesion contour on all slices. The software engineers who were blinded to the patients' clinical, pathological and imaging findings handled the image data, subsequently. Second, gray-level normalization, which is known to minimize the effects of brightness and

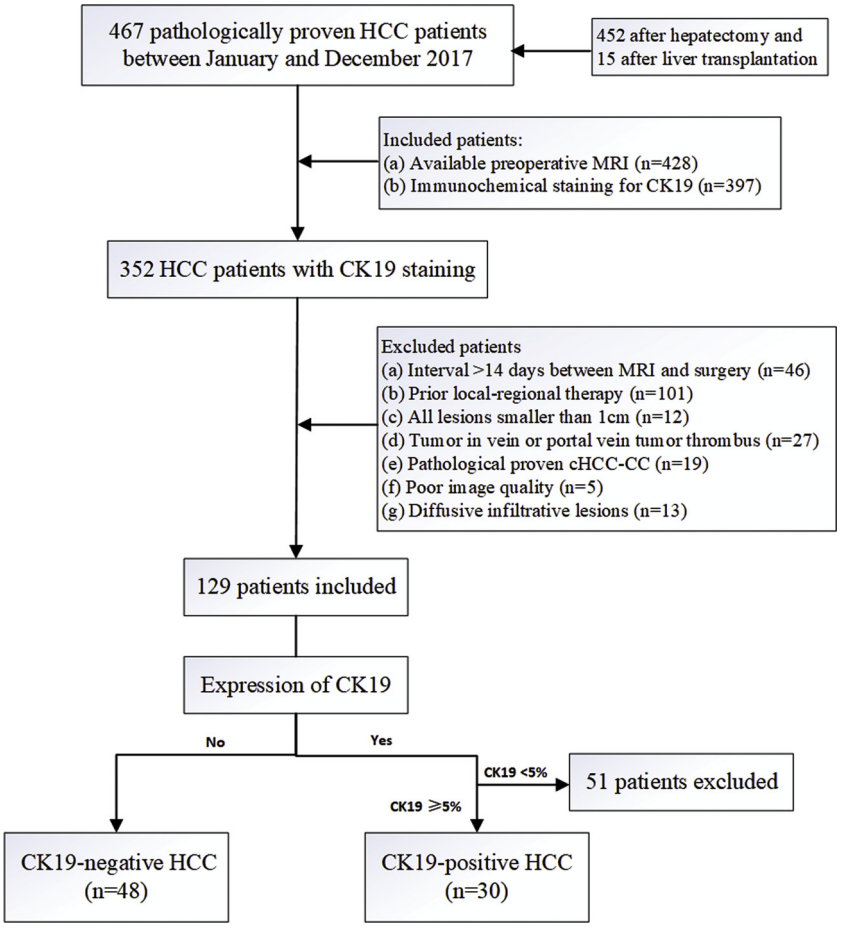

Fig. 1. Flowchart of inclusion and exclusion criteria. HCC, hepatocellular carcinoma; CK19, cytokeratin 19; cHCC-CC, combined hepatocellular carcinoma-cholangiocarcinoma.

Table 1
Parameters of T1-weighted imaging, T2-weighted imaging and diffusion weighted imaging.

Parameter	T1-weighted IP and OP imaging	T1-weighted VIBE imaging	T2-weighted imaging	Diffusion weighted imaging
Repetition time (ms)	123.6	4.53	2658	2807
Echo time (ms)	2.2 and 4.7	2.20	84.7	75.7
Field of view (mm^2)	380 × 290	400 × 280	380 × 360	380 × 300
Matrix	268 × 512	268 × 512	190 × 288	180 × 256
Section thickness (mm)	6.0	3.0	6.0	6.0
Gap (mm)	0	0	1.2	1.2

IP, in-phase; OP, opposed-phase; VIBE, volumetric interpolated breath-hold examination.

contrast variations on the outcome of texture analyses, was conducted by scaling the gray-level values to a designated range [12].

2.5.2. Feature selection

Texture analyses were performed using an in-house software (United Imaging Healthcare, Shanghai, China) that included the intensity, gradient, Gabor wavelet, local binary pattern histogram Fourier (LBP-HF), gray-level co-occurrence matrix (GLCM), and grey level gradient co-occurrence matrix (GLGCM). To enhance the details of the intensity and gradient, we performed local contrast enhancement on the original image to obtain two different enhanced images with a small (7.7 × 7.7 mm^2 kernel size) and a large (35.7 × 35.7 mm^2 kernel size) Gaussian kernel at a standard deviation of 16 [9,13]. Altogether, 345 features were analyzed, including the intensity (n = 117), gradient (n = 96), Gabor wavelet (n = 24), LBP-HF (n = 30), GLCM (n = 33), and the GLGCM (n = 45) features. Overall, the seven conventional sequences (T1WI, T2WI, DWI, ADC map, and dynamic enhanced arterial, portal venous and delayed phase imaging) generated a set of 2415 features.

2.5.3. Classification

The four-fold cross validation and sequential forward floating feature selection strategy were employed to select an optimum subset of features. A linear discriminant analysis was employed and the discriminative features were gradually included and excluded one-by-one until the area under receiver operating characteristic curve (AUC) value no longer increased.

2.6. Statistical analyses

All statistical analyses were performed using SPSS 20.0 (Chicago, IL, USA) and Medcalc software (version 15.0; Mariakerke, Belgium).

Normality of data was tested using the Kolmogorov-Smirnov test, and homogeneity of variance was tested using the Levene method. Statistics were summarized as mean ± standard deviation or median and interquartile range depending on the distribution. The clinicopathological and MR imaging findings were compared between CK19-negative and CK19-positive HCCs, continuous variables were compared with the independent sample *t*-test or Mann-Whitney U test, and categorical variables were compared using Pearson χ^2 test or Fisher's exact test. Factors with a *P* value less than 0.05 at univariate analyses and the top 1 texture character were included into the multivariate model. Multivariate logistic regression analyses were performed using the backward stepwise elimination method to identify the independent predictors. The Hosmer-Lemeshow test was performed to explain the goodness of fit of the multivariate logistic model. Receiver operating characteristic analyses of the significant findings were performed to evaluate their diagnostic performance; AUC, sensitivity, specificity, positive likelihood ratio, and negative likelihood ratio with 95% confidence intervals were calculated. AUCs were compared using the DeLong method. All tests were two sided, and $P < 0.05$ was considered significant.

3. Results

3.1. Patient characteristics

Overall, 78 patients (62 men and 16 women; median age 57.0 years, range 34–77 years) were included in this study. 48 and 30 patients were divided into the CK19-negative and CK19-positive subgroups, respectively. Baseline clinical and pathologic characteristics are shown in Table 2. Serum alpha-fetoprotein (AFP) level of CK19-positive HCCs (mean 2861.7 ng/mL) was higher than CK19-negative HCCs (mean 633.5 ng/mL) overall ($\chi^2 = 6.920$, $P = 0.009$).

3.2. Conventional MR imaging features

Qualitative analysis results are presented in Table 3. At univariate analysis, arterial rim enhancement was more frequently shown in CK19-positive HCCs ($P = 0.002$) (Fig. 2).

At quantitative analysis, the size of CK19-negative and CK19-positive HCCs was not significantly different (3.49 ± 1.33 vs 2.96 ± 1.43 cm, respectively; $t = 1.651$, $P = 0.103$). There were no differences between the two groups in both ADC values (1.526 ± 0.345 vs 1.388 ± 0.349 $\times 10^{-3}$ mm^2/s; $t = 1.715$, $P = 0.09$) and the tumor-to-liver ADC ratio (median 0.89 [interquartile range 0.759, 1.049] vs 0.889 [0.692, 1.026]; $P = 0.372$).

Table 2
Clinical and pathologic characteristics of HCC according to CK19 expression.

	CK19 (-) (n = 48)	CK19 (+) (n = 30)	*P* value
Age (y)†	57.5 ± 10.4	53.7 ± 7.4	0.089
Sex M/F	41(85.4)/7(14.6)	21(70.0)/9(30.0)	0.101
Hepatitis B Y/N	41(85.4)/7(14.6)	29(96.7)/1(3.3)	0.143
Cirrhosis Y/N	29(60.4)/19(39.6)	23(76.7)/7(23.3)	0.139
AFP (ng/mL) ≥400/ < 400	9(18.8)/39(81.2)	14(46.7)/16(53.7)	**0.009***
Lesion Num. Single/Multiple	41(85.4)/7(14.6)	23(76.7)/7(23.3)	0.327
Edmondson-Steiner grade I-II/III-IV	25(52.1)/23(47.9)	11(36.7)/19(63.3)	0.184
Microvascular invasion Y/N	20(41.7)/28(58.3)	14(46.7)/16(53.7)	0.665

Unless otherwise specified, data are numbers of patients/lesions with percentages in parentheses.
HCC, hepatocellular carcinoma; CK19, cytokeratin 19; AFP, alpha-fetoprotein.
*$P < 0.05$.
† Data are mean ± standard deviation.

3.3. MR texture findings

We listed the top 6 texture features with the highest AUC values in Table 4. Among these six features, all top 5 features derived from T2WI and were related to signal intensity (SI), which were all named standard deviation separation (= [SI of the central ROI - SI of the outer 3 mm]/[SI of the central ROI + SI of the outer 3 mm]).

When the top 1–6 texture features were grouped together, no better performance was found in comparison to the top1 (StdSeparation 3D feature alone. Therefore, we selected the top1 (StdSeparation 3D) texture feature as an image biomarker to evaluate CK19 expression.

3.4. Multivariate analysis and the diagnostic performance

At multivariate analysis, serum AFP level ≥400 ng/mL (odds ratio [OR] = 0.204, $P = 0.013$), arterial rim enhancement (OR = 0.074, $P = 0.005$), and the StdSeparation 3D texture character (OR = 2.841, $P = 0.002$) were independent significant variables associated with CK19-positive HCC. The significance level of Hosmer-Lemeshow test was 0.335, suggesting an acceptable goodness of fit of the model.

Diagnostic test characteristics of serum AFP level, arterial rim enhancement, the StdSeparation 3D texture character, and their combinations for predicting CK19-positive HCC are provided in Table 5. The combination of the three indices showed a higher AUC than serum AFP level ($z = 2.988$, $P = 0.0028$), arterial rim enhancement ($z = 4.369$ $P < 0.0001$), and the combination of AFP level and arterial rim enhancement ($z = 2.584$, $P = 0.0098$), while no significantly better than the StdSeparation 3D texture character alone ($z = 1.757$, $P = 0.0788$). When a cutoff value of -0.545 was used, an acceptable discrimination (AUC = 0.765) with both sensitivity (75.86%) and specificity (75.51%) greater than 75% was achieved for the StdSeparation 3D texture character.

4. Discussion

The expression of CK19 is associated with an overall poorer prognosis for HCC, representing an entity separate from ordinary HCC [8,14]. Our study demonstrated that serum AFP level ≥400 ng/mL, arterial rim enhancement, and the StdSeparation 3D texture character were independent variables associated with CK19-positive HCCs. Of all, the StdSeparation 3D texture character improved the discrimination performance of serum AFP level, arterial rim enhancement, as well as their combination; and it showed a comparable diagnostic performance to the combination of all three variables, with both sensitivity and specificity greater than 75%.

In our studies, CK19 positive HCC was associated with elevated serum AFP (≥400 ng/ml), which was also a feature correlated with a poor prognosis, consistent with Durnez et al. [10].

Arterial rim enhancement was more frequently observed in HCCs with CK19 expression, supported by previous studies [3,8]. It is considered a type of target-like morphology, which is more commonly observed in cholangiocarcinoma or metastasis, while uncommonly seen in HCC [15]. This feature may reflect capsule absence, infiltrative growth, presence of microvascular invasion, or rapid growth with central necrosis [16], which was also reported to be associated with poor differentiation, rapid progression and worse prognosis [17,18].

Our study showed that there was no difference in shape of the contour, ADC values and the tumor-to-liver ADC ratio between CK19 positive and CK19 negative HCCs, which differed from the previous report [8], it maybe related to the relatively small sample size. In this study, conventional contrast agent was used for contrast examintion, not hepatocyte specific contrast agent, so we didn't assess the tumor to liver signal intensity ratio and other parameters on hepatobiliary-phase.

According to our results of texture analysis, all top 5 texture features

Table 3
Qualitative MR imaging features of HCC according to CK19 expression.

	CK19 (-) (n = 48)	CK19 (+) (n = 30)	*P* value
Contour smooth/irregular	27(56.3)/21(43.7)	16(53.3)/14(46.7)	0.801
T1WI hypo-/iso-hyperintensity	37(77.1)/11(22.9)	26(86.7)/4(13.3)	0.383
T2WI iso-hypo-/hyperintensity	6(12.5)/42(87.5)	5(16.7)/25(83.3)	0.741
Homogeneity Y/N	4(8.3)/44(91.7)	6(20.0)/24(80.0)	0.171
Target sign on DWI Y/N	9(18.8)/39(81.2)	5(16.7)/25(83.3)	0.816
Arterial rim enhancement Y/N	2(4.2)/46(95.8)	9(30.0)/21(70.0)	**0.002***
Enhancement intensity mild to moderate/marked	35(72.9)/13(27.1)	26(86.7)/4(13.3)	0.173
Enhancement pattern progressive/persistent/degressive/washout	1(2.1)/13(27.1)/6(12.5)/28(58.3)	0(0)/11(36.7)/6(20.0)/13(43.3)	0.395
Enhancing capsule Y/N	35(72.9)/13(27.1)	18(60.0)/12(40.0)	0.234

Data are numbers of lesions with percentages in parentheses.
HCC, hepatocellular carcinoma; CK19, cytokeratin 19; T1WI, T1-weighted imaging; T2WI, T2-weighted imaging; DWI, diffusion weighted imaging.
* $P < 0.05$.

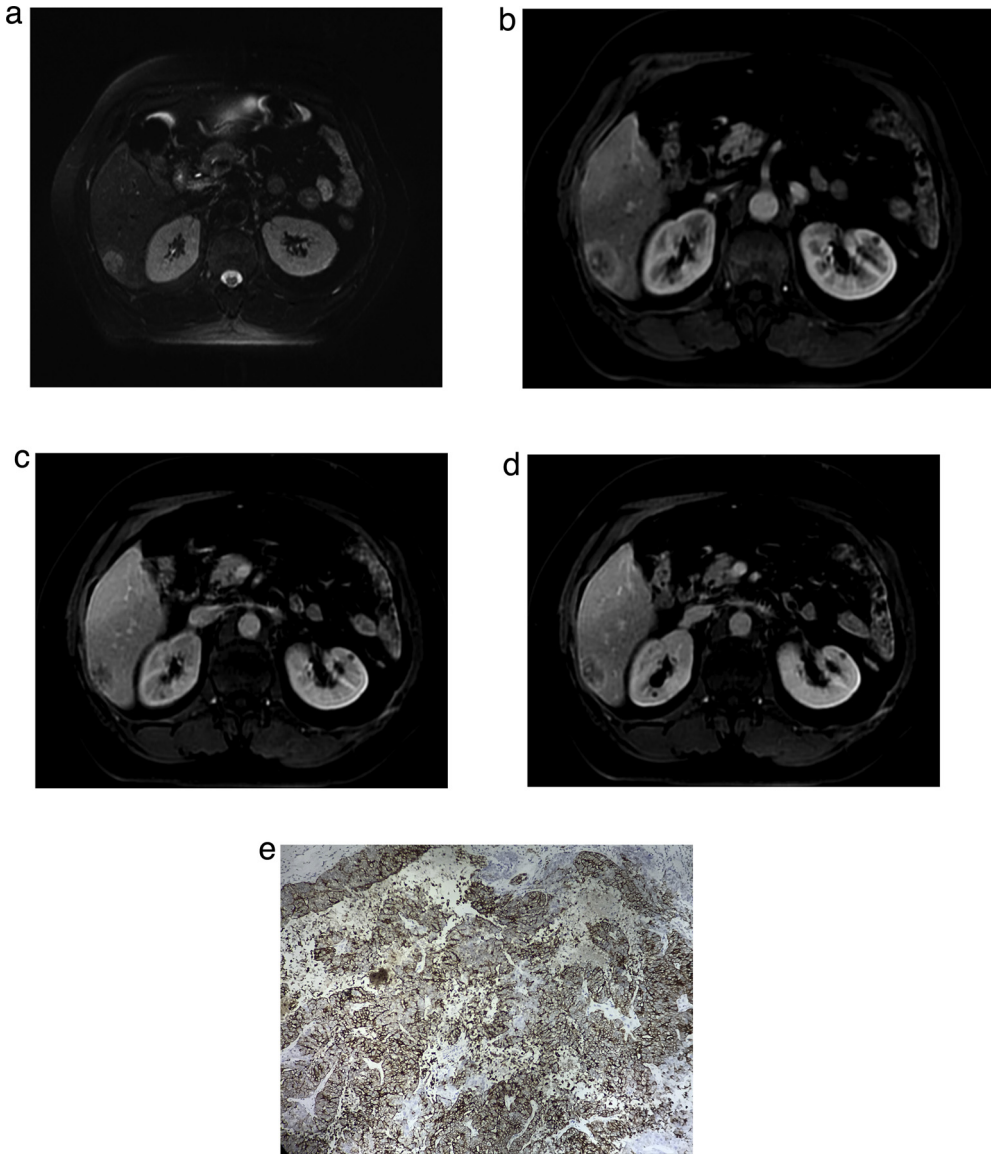

Fig. 2. Cytokeratin 19 (CK19)-positive hepatocellular carcinoma in a 53-year-old man. The mass shows high SI on (a) T2-weighted image, (b)Contrast-enhanced arterial phase image shows a rim enhancement mass. (c) Portal venous and (d)delayed phase images show a wash out enhancement pattern with enhancing capsule. (e) Microscopy (CK19 immunostaining, ×100) shows positive CK19 expression.

Table 4
The top 6 MR texture features with highest AUC values (descending order).

Order	AUC	sequence	Feature group	Calculation image	Feature name
Top1	0.765	T2WI	Intensity	original image	StdSeparation3D_One
Top2	0.736	T2WI	Intensity	LCE2	StdSeparation3D_One
Top3	0.706	T2WI	Intensity	original image	StdSeparation2D
Top4	0.703	T2WI	Intensity	original image	StdSeparation3D_Zdirection
Top5	0.694	T2WI	Intensity	LCE2	StdSeparation2D
Top6	0.688	T1WI	GLGCM	LCE1	GLGCM_SmallGradientStrengths

AUC, area under the curve; LCE1, local contrast enhancement (7.7 × 7.7 mm kernel size); LCE2, local contrast enhancement (35.7 × 35.7 mm kernel size); StdSeparation, the standard deviation separation; GLGCM, grey level gradient co-occurence matrix.

Table 5
Diagnostic performance of the three significant findings and combinations for predicting CK19-positive HCC.

	AUC	Sensitivity(%)	Specificity(%)	LR+ (%)	LR- (%)
AFP ≥400 ng/mL	0.650 (0.533, 0.754)	48.28 (29.4, 67.5)	81.63 (68.0, 91.2)	2.63 (1.3, 5.3)	0.63 (0.4, 0.9)
Arterial rim enhancement	0.635 (0.518, 0.741)	31.03 (15.3, 50.8)	95.92 (86.0, 99.5)	7.60 (1.8, 32.8)	0.72 (0.6, 0.9)
Stdseparation 3D-texture	0.765 (0.655, 0.853)	75.86 (56.5, 89.7)	75.51 (61.1, 86.7)	3.10 (1.8, 5.3)	0.32 (0.2, 0.6)
AFP + rim enhancement	0.740 (0.628, 0.832)	65.52 (45.7, 82.1)	77.55 (63.4, 88.2)	2.92 (1.6, 5.2)	0.44 (0.3, 0.8)
All three parameters	0.844 (0.744, 0.916)	93.10 (77.2-99.2)	61.22 (46.2, 74.8)	2.40 (1.7, 3.5)	0.11 (0.03, 0.4)

Data in parentheses are 95% confidence intervals.
CK19, cytokeratin 19; HCC, hepatocellular carcinoma; AUC, area under the curve; LR, likelihood ratio; AFP, alpha-fetoprotein.

came from T2WI and calculated the standard deviation separation of SI. Thus, the SI discrepancy of the internal and external part of lesions may be different between CK19-positive and CK19-negative HCCs. It has been proved that inhomogeneity on T2WI was more commonly seen in cholangiocarcinoma than HCC [19]; and the CK19-positive HCC was regarded to be closer in lineage to biliary cells than hepatocytes, which may reveal more similarity with cholangiocarcinoma [10]. However, conventional lesion homogeneity judgement on T2WI showed no significant differences. We considered that texture analysis allowed objective assessment of lesion heterogeneity beyond what was possible with subjective visual interpretation [9].

In our study, the diagnostic performance of StdSeparation 3D texture character alone was comparable to the combination of all top 6 features, and was an independent variables for predicting CK19-positive HCCs, which can improve the diagnostic efficiency of conventional features of AFP level and arterial rim enhancement. For future directions, an objective tool like texture analysis, which would allow a ROI placement and quantitative texture feature measurement, as signal intensity or Hounsfield unit, is expected [9]. This may allow radiologists to obtain additional and more robust data from studies routinely performed. Thus, we considered MR texture analysis, especially the StdSeparation 3D texture character, a promising imaging biomarker for CK19-positive HCC prediction, which would provide radiologists with a more objective assessment and improve the diagnostic confidence.

Our study has several limitations. First, selection bias was inevitable because of the retrospective design. CK19 staining was not performed consecutively for all surgically proven HCCs. Second, the sample size was relatively small, considering the multiple texture characters. Third, ROI analysis was not performed in the areas specifically expressing CK19. ROI was drawn including the whole lesion as large as possible, and we believed that our data obtained was sufficient to demonstrate the overall features of HCC expressing CK19 [3]. Fourth, studies have proved that hepatobiliary-phase Gd-EOB-DTPA-enhanced MRI may be helpful to predict CK19-positive HCCs [3,8]. However, we used gadopentetate dimeglumine in this study; thus, comparison with existing predictive models was lacking. After all, large, multicenter, prospective studies are needed to validate texture analysis as a clinical tool.

In conclusion, serum AFP level ≥400 ng/mL, arterial rim enhancement, and the StdSeparation 3D texture character were independently associated with CK19-positive HCCs. Of all, the StdSeparation 3D MR texture character may be a reliable imaging biomarker, which can improve the diagnostic performance of conventional features of AFP level and arterial rim enhancement.

References

[1] A. Forner, M. Reig, J. Bruix, Hepatocellular carcinoma, Lancet (London, England) 391 (10127) (2018) 1301–1314.
[2] L.A. Torre, F. Bray, R.L. Siegel, J. Ferlay, J. Lortet-Tieulent, A. Jemal, Global cancer statistics, 2012, CA Cancer J. Clin. 65 (2) (2015) 87–108.
[3] H.T. Jeong, M.J. Kim, Y.E. Kim, Y.N. Park, G.H. Choi, J.S. Choi, MRI features of hepatocellular carcinoma expressing progenitor cell markers, Liver Int. 32 (3) (2012) 430–440.
[4] H. Kim, G.H. Choi, D.C. Na, E.Y. Ahn, G.I. Kim, J.E. Lee, J.Y. Cho, J.E. Yoo, J.S. Choi, Y.N. Park, Human hepatocellular carcinomas with "Stemness"-related marker expression: keratin 19 expression and a poor prognosis, Hepatology (Baltimore, Md.) 54 (5) (2011) 1707–1717.
[5] M. Takano, K. Shimada, T. Fujii, K. Morita, M. Takeda, Y. Nakajima, A. Nonomura, N. Konishi, C. Obayashi, Keratin 19 as a key molecule in progression of human hepatocellular carcinomas through invasion and angiogenesis, BMC Cancer 16 (1) (2016) 903.
[6] K. Tsuchiya, M. Komuta, Y. Yasui, N. Tamaki, T. Hosokawa, K. Ueda, T. Kuzuya, J. Itakura, H. Nakanishi, Y. Takahashi, M. Kurosaki, Y. Asahina, N. Enomoto, M. Sakamoto, N. Izumi, Expression of keratin 19 is related to high recurrence of hepatocellular carcinoma after radiofrequency ablation, Oncology 80 (3-4) (2011) 278–288.
[7] G.E. Chung, J.H. Lee, J.H. Yoon, S.J. Myung, K. Lee, J.J. Jang, J.M. Lee, S.H. Kim, K.S. Suh, Y.J. Kim, H.S. Lee, Prognostic implications of tumor vascularity and its relationship to cytokeratin 19 expression in patients with hepatocellular carcinoma, Abdom. Imaging 37 (3) (2012) 439–446.
[8] S.Y. Choi, S.H. Kim, C.K. Park, J.H. Min, J.E. Lee, Y.H. Choi, B.R. Lee, Imaging features of gadoxetic acid-enhanced and diffusion-weighted MR imaging for identifying cytokeratin 19-positive hepatocellular carcinoma: a retrospective observational study, Radiology 286 (3) (2018) 897–908.
[9] M.G. Lubner, A.D. Smith, K. Sandrasegaran, D.V. Sahani, P.J. Pickhardt, CT texture analysis: definitions, applications, biologic correlates, and challenges, Radiographics 37 (5) (2017) 1483–1503.
[10] A. Durnez, C. Verslype, F. Nevens, J. Fevery, R. Aerts, J. Pirenne, E. Lesaffre, L. Libbrecht, V. Desmet, T. Roskams, The clinicopathological and prognostic relevance of cytokeratin 7 and 19 expression in hepatocellular carcinoma. A possible progenitor cell origin, Histopathology 49 (2) (2006) 138–151.
[11] H. Wang, C. Yang, S. Rao, Y. Ji, J. Han, R. Sheng, M. Zeng, MR imaging of hepatocellular adenomas on genotype-phenotype classification: a report from China, Eur. J. Radiol. 100 (2018) 135–141.
[12] D.L. Campbell, H. Kang, S. Shokouhi, Application of Haralick texture features in brain [(18)F]-florbetapir positron emission tomography without reference region normalization, Clin. Interv. Aging 12 (2017) 2077–2086.
[13] T. Messay, R.C. Hardie, S.K. Rogers, A new computationally efficient CAD system for pulmonary nodule detection in CT imagery, Med. Image Anal. 14 (3) (2010) 390–406.
[14] S. Aishima, Y. Nishihara, Y. Kuroda, K. Taguchi, T. Iguchi, A. Taketomi, Y. Maehara, M. Tsuneyoshi, Histologic characteristics and prognostic significance in small hepatocellular carcinoma with biliary differentiation: subdivision and comparison

with ordinary hepatocellular carcinoma, Am. J. Surg. Pathol. 31 (5) (2007) 783–791.
[15] K.M. Elsayes, J.C. Hooker, M.M. Agrons, A.Z. Kielar, A. Tang, K.J. Fowler, V. Chernyak, M.R. Bashir, Y. Kono, R.K. Do, D.G. Mitchell, A. Kamaya, E.M. Hecht, C.B. Sirlin, Version of LI-RADS for CT and MR Imaging: an update, Radiographics 37 (7) (2017) (2017) 1994-2017.
[16] C. An, D.W. Kim, Y.N. Park, Y.E. Chung, H. Rhee, M.J. Kim, Single hepatocellular carcinoma: preoperative MR imaging to predict early recurrence after curative resection, Radiology 276 (2) (2015) 433–443.
[17] A.S. Kierans, P. Leonardou, P. Hayashi, L.M. Brubaker, M. Elazzazi, F. Shaikh, R.C. Semelka, MRI findings of rapidly progressive hepatocellular carcinoma, Magn. Reson. Imaging 28 (6) (2010) 790–796.
[18] H. Imamura, Y. Matsuyama, E. Tanaka, T. Ohkubo, K. Hasegawa, S. Miyagawa, Y. Sugawara, M. Minagawa, T. Takayama, S. Kawasaki, M. Makuuchi, Risk factors contributing to early and late phase intrahepatic recurrence of hepatocellular carcinoma after hepatectomy, J. Hepatol. 38 (2) (2003) 200–207.
[19] R. Kim, J.M. Lee, C.I. Shin, E.S. Lee, J.H. Yoon, I. Joo, S.H. Kim, I. Hwang, J.K. Han, B.I. Choi, Differentiation of intrahepatic mass-forming cholangiocarcinoma from hepatocellular carcinoma on gadoxetic acid-enhanced liver MR imaging, Eur. Radiol. 26 (6) (2016) 1808–1817.